Assessing zinc from a nail clipping using mono-energetic portable X-ray fluorescence

David E.B. Fleming[1], Samantha L. Crook[1], and Colby T. Evans[1].

[1]Physics Department, Mount Allison University, Sackville, NB, Canada

Corresponding Author e-mail: dfleming@mta.ca; phone: (506) 364-2584

Abstract

A mono-energetic X-ray beam from a portable X-ray fluorescence device was used to excite characteristic X-rays from zinc in a series of nail clipping phantoms. Twenty nail clipping phantoms having equal zinc concentrations of ~40 μg/g, but with different physical characteristics, were measured individually for 300 s using a small diameter (~1 mm) X-ray beam. Energy spectra obtained from the measurements were analyzed using PyMca software. Zinc signal size varied widely between the different clippings, with a relative standard deviation of 41% observed in the combined signal from zinc Kα and Kβ characteristic X-rays. Three different normalization approaches were introduced to account for variation in the amounts of sample interrogated by the X-ray beam. All three approaches produced similar results, and successfully reduced the relative standard deviation to between 12 – 13%. A clear trend was still observed, however, between the normalized zinc signal and the thickness of clipping measured. To account for this effect, normalized signals were adjusted to calculate "thickness-corrected" values. The relative standard deviation of these thickness-corrected values was 6.2%. Reproducibility of measurement from individual clippings was excellent, with relative standard deviations on the order of 1%, with or without normalization. Overall, this new method of measuring zinc in nail shows promise for the assessment of zinc status in humans using a portable device. The method is sensitive, rapid, and requires only a single nail clipping.

Keywords: mono-energetic X-ray; portable X-ray fluorescence; zinc; nail clippings; biomarker

1. Introduction

The potential for measurement of trace elements in human nail and nail clippings using portable X-ray fluorescence has received growing attention in recent years. Feasibility studies using phantom nail materials have been presented for arsenic and selenium (Roy et al., 2010; Gherase and Fleming, 2011; Fleming et al., 2017), manganese and zinc (Fleming et al., 2013; Fleming et al., 2018), and chromium (Fleming and Ware, 2017). Applications with real human nails and nail clippings have followed, with investigations considering iron, zinc, and other elements (Figueroa et al., 2014), arsenic (McIver et al., 2015), and manganese and lead (Specht et al., 2018). Portable (or small-scale) X-ray fluorescence systems can generally not provide the sensitivity of elemental detection available from a "gold standard" method such as inductively coupled plasma mass spectrometry. Nonetheless, portable X-ray fluorescence offers a number of advantages making it an attractive option for use with nail clippings.

Chief among the advantages of a portable X-ray fluorescence approach to analysis of nails is the ability to make measurements in a variety of settings and provide results quickly (Fleming et al., 2017). Portable X-ray fluorescence systems are mobile and can operate from battery power if necessary. The measurement itself is straightforward and rapid, requiring little sample preparation. Likewise, the analysis of data can be performed quickly using a notebook computer. These features allow results to be returned to individuals without the long delays usually associated with tests performed at distant labs. Similar to inductively coupled plasma mass spectrometry, multiple elements can be measured at the same time using X-ray fluorescence (Fleming et al., 2017). Cost of operation is low for portable X-ray fluorescence systems, with relatively modest initial purchase expenses, and little maintenance required (Specht et al., 2018).

One development, in particular, has recently advanced capabilities for using portable X-ray fluorescence to assess elemental concentrations in nail clipping samples. The introduction of doubly curved crystal optics has provided the ability to use a small-focus, high intensity, mono-energetic X-ray beam for portable X-ray fluorescence. The mono-energetic aspect allows for the selection of a specific energy of irradiation, which is more efficient for exciting characteristic X-rays from a certain element or suite of elements. This dramatically improves measurement precision compared to conventional X-ray fluorescence techniques, which rely on excitation from a broad range of energies obtained via Bremsstrahlung radiation. For example, the mono-energetic approach using a measurement time ~3 minutes provided a minimum detection limit of less than 1 μg/g for arsenic and selenium in a single clipping (Fleming et al., 2017). Furthermore, the very small beam diameter of ~1 mm resulting from the optics approach (Guimãraes et al., 2016) has the benefit of allowing the entire beam area to interrogate a single nail clipping (Fleming et al., 2017). This maximizes elemental signal strength, and reduces the large variations in signal introduced by differences in sample size from collections of multiple clippings (Fleming et al., 2013).

Zinc represents one of the most promising elements for study in nail clippings, and portable x-ray fluorescence could play an important role in its measurement. Zinc deficiency is a widespread medical issue (Wessells and Brown, 2012), with serious implications for human growth and development, and for the function of the immune, central nervous, and gastrointestinal systems (Hambidge, 2000). Diagnosis of zinc deficiency, however, is often impeded by the lack of a reliable biomarker. In an expert panel review, zinc concentration in nail was recently described as an "emerging biomarker" for assessing zinc status (King et al., 2016). Zinc levels in nail have been demonstrated to reflect zinc nutriture in humans, making the ability to measure zinc in nail with a mobile system a promising development (Fleming et al., 2018). A previous study using a conventional portable x-ray fluorescence system to assess zinc in nail clipping phantoms indicated a detection limit of ≤ 1 μg/g for a collection of nail clippings having a combined mass of 100 mg (Fleming et al., 2013). However, the technique used in that study involved a relatively large incident X-ray beam, and demonstrated a strong signal dependence on the combined mass of the sample. These features required multiple clippings to be used for each measurement and the introduction of a sample mass correction (Fleming et al., 2013). More recently, it was suggested that Compton scatter signal be used to normalize elemental signals from a conventional portable X-ray fluorescence system, potentially removing the necessity of correcting for the size or thickness of clippings (Specht et al., 2018).

In the current study, we examine for the first time the use of a narrow beam, mono-energetic portable X-ray fluorescence system for detecting zinc in nail clipping phantoms. Similar to recent work involving arsenic and selenium (Fleming et al., 2017), only single clippings will be measured in this study (as opposed to collections of multiple clippings). The use of a single clipping simplifies the measurement procedure, and makes the method more practical for potential applications involving nail clippings from people. (If, however, only small fragments or chips of nail are available, a collection from a given individual may still be required.) The sensitivity of portable X-ray fluorescence techniques for nail clippings has been established (Fleming et al., 2013; Fleming et al., 2017), and therefore the focus of the current paper is not on detection limits or signal response as a function of concentration. The individual nail clipping phantoms used in this study were all produced from the same original source material, and therefore contain roughly equal concentrations of zinc. However, variations in zinc measurement signal may arise from differences in the physical characteristics of the individual clippings. The degree of variation in signal between clippings will therefore be studied in the current paper. In addition, various normalization techniques will be tested to assess different possible approaches to data analysis, in order to minimize any such variation.

2. Methods

The samples used for this study were made to simulate human nail clippings, and will be referred to here as "nail clipping phantoms". The method of creating the nail clipping phantoms has been described previously (Fleming et al., 2013). Briefly, a commercially available liquid resin (Bondo Corp.; Atlanta, GA) was used, and dosed with zinc from an atomic absorption spectrometry standard solution (Sigma-Aldrich; Oakville, ON). After adding the zinc solution and mixing, a hardening solution was introduced (Bondo Corp.; Atlanta, GA). While still in its liquid form, the zinc-dosed resin was poured out as a thin sheet measuring approximately 25 mm x 25 mm. This sheet of resin was allowed to dry to a solid form over 48 hours. Commercial nail clippers were then used on the sheet to create a large number of nail clipping phantoms. These clippings were of a variety of sizes, shapes, and thicknesses, similar to what would be expected from real nail clippings. The concentration of zinc in the clipping phantoms, as calculated from the amount of atomic absorption spectrometry standard used in their construction, was ~40 μg/g.

Measurement of individual clipping phantoms was performed using an HD Mobile X-ray fluorescence system (X-ray Optical Systems; East Greenbush, NY). The HD Mobile unit used in this study was similar to an apparatus used in another recent study involving clipping phantoms (Fleming et al., 2017), but differed in that it was operated in a benchtop test stand mode (as opposed to a transporter/carrying case mode). The operating characteristics of the HD Mobile system included use of a molybdenum X-ray target, an X-ray tube current of 200 μA, and a tube voltage of up to 50 kV. The mono-energetic beam was selected at 17.4 keV, corresponding to the molybdenum Kα energy. This energy was the best available match for the excitation of X-ray fluorescence from zinc, which has a K-edge of 9.7 keV. Although a higher efficiency of exciting characteristic X-rays from zinc could be achieved using a different X-ray target material and beam energy, the use of a molybdenum target is the most practical option for exciting a wide range of elements using a single system. The radiation detector was a silicon drift detector, having a diameter of 25 mm.

Twenty individual nail clipping phantoms were selected for measurement, representing a range of clipping sizes and thicknesses. Each clipping was assessed for its mass (Adventurer Pro AV264 balance, Ohaus Co.; Pine Brook, NJ) and thickness (digital caliper, Princess Auto; Winnipeg, MB), and photographed to assess surface area (ImageJ software, NIH; Bethesda, MD). For each of the twenty clippings, an X-ray fluorescence measurement was made for 300 s (real time). The resulting energy spectrum, representing recorded counts as a function of energy, was saved and analyzed using PyMca software (ESRF; Grenoble, France). PyMca was developed at the European Synchrotron Research Facility for X-ray fluorescence analysis (Solé et al., 2007), and its use with spectra from portable X-ray fluorescence has provided results with high levels of accuracy (de Viguerie et al., 2009). From the Peaks tab in the fit configuration window of PyMca, iron, cobalt, nickel, copper, and zinc were selected for spectral fitting. For each of these elements, the fitting was performed separately for the Kα and Kβ characteristic X-ray transitions. The software accounted for all possible Kα and Kβ characteristic X-ray transitions, along with the associated escape peaks. The fit to the data as a whole, and the net signal contributions from zinc in particular, were reviewed and saved from each individual clipping. For each clipping, zinc Kα signal, uncertainty in zinc Kα signal, zinc Kβ signal, and uncertainty in zinc Kβ signal were recorded from the output of the Table tab in the advanced fit window of PyMca. These signals represented spectral peak areas, in units of counts x keV.

Zinc signal by itself was not expected to be a perfect indicator of zinc concentration (defined as the mass of zinc per mass of sample), since the intensity of the zinc signal could depend in part on the *amount* of sample interrogated by the incident X-ray beam. Variations in sample size and thickness can affect the amount of sample interrogated by the beam. Additionally, variations in sample size and thickness can introduce small differences in detector dead time and count results. For these reasons, different methods of normalizing the "zinc signal" to a "sample signal" were attempted, in order to provide the best possible indicator of zinc concentration from an X-ray fluorescence measurement. Three different techniques were examined as possible approaches for normalizing against a "sample signal": (1) use of the coherent scatter signal obtained from a sample, as determined from counts recorded under a detection peak centered at 17.4 keV (resulting from coherent scatter of molybdenum Kα characteristic X-rays); (2) use of the Compton and coherent scatter signals obtained from a sample, as determined from the counts recorded from 14 keV to 18 keV; (3) use of the signal over the entire spectrum obtained from a sample, as determined from the counts recorded over all available energies.

The coherent scatter approach to normalization has been used in other X-ray fluorescence applications, most notably with the assessment of lead concentration in bone (Somervaille et al., 1985). The current application, however, does not share the particular advantage of the bone lead technique where both the lead signal and the coherent signal result directly from essentially the same initial photon fluence. As noted above, a Compton scatter approach to normalization has recently been used for the measurement of manganese and lead concentrations in nail clippings (Specht et al., 2018). Our decision to use a range of energies (14 keV-18 keV) to model both the Compton and coherent contributions was based on the complicated shape of the energy spectrum over this range. Finally, the use of the total number of counts from the entire spectrum accounted for the full range of detections received from the sample, and represented the simplest of the three approaches to normalization investigated.

From the twenty clipping measurements, the average zinc signal, sample standard deviation of the zinc signal, and relative standard deviation of the zinc signal were determined. The same three parameters (average, sample standard deviation, and relative standard deviation) were also calculated using the three *normalized* quantities described above: (1) zinc signal / sample signal (as determined from the coherent scatter); (2) zinc signal / sample signal (as determined from the Compton and coherent scatter); (3) zinc signal / sample signal (as determined from the total number of counts over the entire spectrum). Since each of the twenty clipping phantoms was expected to have approximately the same concentration of zinc (40 μg/g), a smaller relative standard deviation indicates a better method of assessing concentration.

Finally, to examine the reproducibility of measurement using the various approaches outlined above, two individual clippings were selected for repeat measurement. Both of the selected clippings were measured for ten additional 300 s (real time) trials. The selected clippings were not moved between trials so that, as far as possible, measurement conditions could be kept the same. It was expected that the relative standard deviation of these results would be reduced compared to the cases involving the twenty separate clippings. The individual clipping reproducibility trial results were reviewed to provide further information on the different methods used in this study.

3. Results

The individual nail clipping phantoms had a range of different physical characteristics. The masses of the single clippings ranged from 4.7 ± 0.5 mg to 47.4 ± 0.5 mg, with a median mass of 14.5 mg. Variations in thickness were not as pronounced, but still evident. The thickness of individual clippings ranged from 0.30 ± 0.05 mm to 1.20 ± 0.05 mm, with a median value of 0.80 mm. Likewise, the surface area of the clippings as measured from one face ranged from 21 ± 1 mm^2 to 75 ± 2 mm^2, with a median result of 35 mm^2. This degree of physical variation was broadly consistent with that expected from a collection of human nail clippings. Toenail clipping masses in one study involving children ranged from 5 mg to 151 mg (Pearce et al., 2010), while another study with adults reported an average total clipping mass (from all ten toes) of 99 mg, implying an average single clipping mass of ~10 mg (Specht et al., 2018). A further study involving human nail found healthy nails to range in clipping thickness from 0.3 mm to 1 mm (Baraldi et al., 2015).

Typical energy spectra, obtained from two of the twenty clippings assessed by X-ray fluorescence in this study, are provided in Figure 1. Figure 1 (a) presents the PyMca fit to the energy spectrum between 6.0 keV and 10.0 keV obtained from clipping # 5, while Figure 1 (b) presents the fit to the spectrum from clipping # 8 over the same energy range. In both cases, the red line represents the PyMca fit to various elemental signals, while the green line represents the PyMca fit to the background continuum. The data points themselves (in black) are largely obscured by the fitting lines. While this feature highlights the good fit provided to the data when using the PyMca software, it does make a visual comparison between the data and the fit somewhat difficult. The reduced chi square value over the 6.0 – 10.0 keV interval was 2.0 for clipping # 5, and 2.3 for clipping # 8. The signal from zinc is clearly evident in both cases, with energy peaks centered at 8.6 keV (Kα characteristic X-rays) and 9.6 keV (Kβ characteristic X-rays). It is notable that the zinc signals from clipping # 5 are significantly larger than those from clipping # 8. The zinc Kα signal from clipping # 5 has an area of 711 ± 6, while the zinc Kα signal from clipping # 8 has an area of 480 ± 3. Likewise, the zinc Kβ signal from clipping # 5 has an area of 110 ± 2, while the zinc Kβ signal from clipping # 8 has an area of 76 ± 2. This aspect of the results is discussed in more detail below. Other elements shown in the spectra are iron (6.4 keV and 7.1 keV), cobalt (6.9 keV and 7.6 keV), nickel (7.5 keV and 8.3 keV), and copper (8.0 keV and 8.9 keV). The relatively small signals from iron, nickel, and copper result from the excitation of components within the benchtop stand and system housing. The large signal from cobalt is attributed to its presence in the materials used to create the nail clipping phantoms (Studinski et al., 2005; Fleming and Gherase, 2007). The background continuum is relatively small and flat over the energy range of interest.

For each of the twenty clipping phantoms analyzed, the zinc Kα signal area and the zinc Kβ signal area obtained from the PyMca fittings are shown independently in Figure 2. Generally speaking, the relative uncertainties returned from PyMca for the Kα areas tended to be larger than the relative uncertainties for the Kβ areas. This is believed to be related to the slightly more complicated shape of the background continuum in the vicinity of Kα peak. It is clear from the results in Figure 2 that the ratio of zinc Kα signal to zinc Kβ signal was very consistent from clipping to clipping. The values themselves, however, varied considerably between clippings. The relative standard deviation of the Kα signal results was 41.4%, and the relative standard deviation of the Kβ signal results was 41.5%. For each clipping, the Kα and Kβ signals were summed together to arrive at a single consolidated zinc signal area. These consolidated zinc signals ranged from 155 ± 2 to 821 ± 6. The average consolidated zinc signal from the twenty clipping measurements was 479.7, while the sample standard deviation was 198.4. The relative standard deviation of the zinc signal from the twenty clippings was therefore 41.4%, representing a considerable amount of variation. However, the variation in results between clippings was greatly reduced by introducing a normalization term to the analysis. Table 1 summarizes these results, when using the three different normalization conditions described in the Methods: (1) zinc signal / sample signal (as determined from the coherent scatter); (2) zinc signal / sample signal (as determined from the Compton and coherent scatter); (3) zinc signal / sample signal (as determined from the total number of counts over the entire spectrum). Introducing normalization reduced the relative standard deviation by more than a factor of three, to between 12% - 13%.

Notably, an inspection of the overall results as a function of the physical properties (mass, thickness, and surface area) of the clipping phantoms indicated one clear and obvious relationship between variables. As shown in Figure 3, the normalized zinc signal / sample signal (as determined from the total number of counts over the entire spectrum) from the clippings demonstrated a strong negative correlation with clipping thickness. This negative relationship was evident from both the zinc Kα and zinc Kβ results, but was especially strong with the Kα results. In both cases, a best fit linear relationship was introduced as a simple means of modeling this effect. For the zinc Kα signal / sample signal as a function of clipping thickness, the correlation coefficient was $r = -0.87$. For the zinc Kβ signal / sample signal as a function of clipping thickness, the correlation coefficient was $r = -0.77$.

The two clippings selected for the analysis of reproducibility, with ten repeat measurements performed under identical conditions, were clipping # 5 and clipping # 8. In both cases, the variation in results between trials was minimal under all conditions of analysis. For clipping # 5, the relative standard deviation of the zinc signal (alone) was 0.9%. When the normalization conditions were introduced, the relative standard deviations of the results were 1.0% (when using the coherent scatter as the normalization condition), 1.0% (when using the Compton and coherent scatter), and 1.0% (when using the entire spectrum). For clipping # 8, the relative standard deviation of the zinc signal (alone) was 1.3%. When the normalization conditions were introduced, the relative standard deviations of the results were 1.3% (when using the coherent scatter as the normalization condition), 1.3% (when using the Compton and coherent scatter), and 1.3% (when using the entire spectrum). In the case of a 1.3% result for relative standard deviation, this corresponds to a standard deviation of 0.52 μg/g, which is useful as an indicator of the sensitivity of the method.

4. Discussion

It is evident from Figure 1 that both the Kα and Kβ characteristic X-ray signals from zinc are easily detected from a 300 s measurement of a single clipping having a zinc concentration of ~40 μg/g. Notably, the concentrations of zinc expected in real human nail clippings are much higher than this level. A review of zinc fingernail concentrations from 17 different human population studies found the vast majority of population means falling between 100 μg/g and 150 μg/g (Fleming et al., 2018). The mono-energetic portable X-ray fluorescence method described in this paper is therefore feasible for application to human populations, given the concentrations of zinc expected in real nail clippings. Real nail clippings would also result in additional signal contributions from elements such as iron, nickel, and copper. These elements are expected to be present in relatively low concentrations (Rodushkin and Axelsson, 2000), and are not anticipated to significantly affect the fitting of the zinc peaks. The focus of the current study was to investigate the variability in results between different clippings when measuring a constant zinc concentration, and assess possible methods to reduce this variability in measurement.

Considering that all of the phantom nail clippings used in this study originated from the same resin sheet having a zinc concentration ~40 μg/g, the amount of variation noted in zinc signal from clipping to clipping was substantial. The relative standard deviation in zinc signal over measurements from twenty different clipping phantoms was 41% (Figure 2). This wide degree of variation highlighted the necessity of introducing a normalization term to account for the different amounts of material interrogated by the X-ray beam from measurement to measurement. In the current study, three different normalization techniques were investigated. These normalization approaches used either the coherent scatter signal, the Compton and coherent scatter signal, or the signal from the entire detected energy spectrum. All three techniques produced similar results, showing relative standard deviations over the twenty clipping measurements of between 12 – 13%. Of the three, the approach using the signal from the entire spectrum provided the lowest relative standard deviation (12.1%) and represented the simplest method to implement. This approach is therefore indicated as a reasonable choice for future applications involving mono-energetic portable X-ray fluorescence measurements of zinc in nail clippings. All three normalization techniques, however, should be considered and reviewed in future work using real nail clippings spanning a range of zinc concentrations.

The observation of a strong negative correlation between normalized zinc signal and clipping thickness (Figure 3) was possibly related to self-attenuation of the zinc signal emerging from the clipping. Since the characteristic X-ray signals from zinc (originating at 8.6 keV for the Kα and 9.6 keV for the Kβ) are relatively low in energy, the strength of the zinc signal received by the detector will plateau as clipping thickness increases (Ichikawa and Nakamura, 2016). However, with the values of clipping thickness used in this study, the signal related to the amount of material interrogated (originating with the higher energy 17.4 keV Kα X-ray of molybdenum) will continue to increase as a function of thickness. The ratio of the two signals (zinc / amount of material) therefore correlates in a negative sense with sample thickness. Here, we have approximated this relationship using a simple linear equation with a negative slope. A similar negative correlation between normalized signal and thickness was not apparent from the study of Specht et al. (2018). It is difficult to be certain as to why this observation emerged in the current study, but could be related to the use of a mono-energetic X-ray beam.

Based on this finding, it seemed reasonable to account for the effect of clipping thickness, and calculate a normalized zinc signal adjusted for variations in thickness. Toward this end, the Kα and Kβ normalized zinc signals (entire spectrum normalization approach) were adjusted to calculate “thickness-corrected” values for each clipping. Calculations were performed to provide results “corrected” to the values expected had all of the clippings been 0.80 mm in thickness (the median thickness of the samples). This correction was calculated using the slopes from the two linear relationships provided in Figure 3. The results from these thickness-corrected Kα and Kβ normalized signals were then summed, and analyzed in the same way as the previously described results. The thickness-corrected values produced an average result of 0.007202, a sample standard deviation of 0.000448, and a relative standard deviation of 6.2%. When compared with results from the final column of Table 1, it is evident that accounting for clipping thickness served to reduce the relative standard deviation of results by nearly a factor of two.

Notably, the ratio of the zinc Kα area to the zinc Kβ area obtained from the twenty clippings was also found to correlate with clipping thickness (Figure 4). This observation is a consequence of differential attenuation of the zinc Kα and zinc Kβ X-ray energies as a function of clipping thickness. With increasing thickness, the lower energy Kα X-rays (8.6 keV) will be more strongly attenuated, relative to the higher energy Kβ X-rays (9.6 keV). Indeed, since Kα detections make up the bulk of the overall zinc signal, this effect may contribute in part to the observation of lower normalized zinc signals as a function of clipping thickness. This feature also suggests that the Kα/Kβ ratio in itself could provide a useful indication of clipping thickness, and perhaps be used to correct the overall zinc signal as outlined above. Some caution, however, is in order before adopting such an approach, especially in light of the one anomalous data point (resulting from a thickness of 1.0 mm) evident in Figure 4.

From the repeated measurement trials using the same two clippings (clipping # 5 and clipping # 8), it was clear that the reproducibility of zinc signal was excellent. Additionally, contrary to the results obtained from measurements across the twenty different clippings, introducing a normalization term did not have much effect on the degree of variation. The relative standard deviation of the zinc signal, with or without normalization, was consistently ~1% from clipping # 5 and ~1.3% from clipping # 8. These results suggest that some portion of the larger variability (6.2%) observed from measurement of zinc across the twenty clippings originated from actual differences in zinc concentration from clipping to clipping. This is not surprising given the small beam size used in this study, capable of detecting local variations in concentration over small spatial scales.

Future work will apply the mono-energetic portable X-ray fluorescence technique described in this study with nail clippings obtained from a human population. It will be important to validate the method using real nail clippings having a range of zinc concentrations, along with a variety of shapes and sizes. This could be accomplished through a comparison of X-ray fluorescence nail clipping results with those from a "gold standard" technique such as inductively coupled plasma mass spectrometry. Special attention should be directed toward the thickness-related effects demonstrated in this paper, to see whether they are also evident in measurements of real nail clippings. Given the potential advantages of a rapid, mobile, and cost effective system for assessing zinc status from nail clippings, the mono-energetic portable X-ray fluorescence approach could have far-reaching implications for population health.

Acknowledgements

This work was supported by a Discovery Grant from the Natural Sciences and Engineering Research Council of Canada.

Tables

Result	Normalization condition		
	Coherent scatter	Compton and coherent scatter	Entire spectrum
Average	0.08382	0.007671	0.007233
Sample standard deviation	0.01061	0.000951	0.000876
Relative standard deviation	12.7 %	12.4 %	12.1 %

Table 1. Summary of zinc measurement results obtained from twenty nail clipping phantoms using three different normalization conditions.

References

Baraldi, A., Jones, S.A., Guesné, S., Traynor, M.J., McAuley, W.J., Brown, M.B., and Murdan, S. (2015). Human nail plate modifications induced by onychomycosis: implications for topical therapy. *Pharmaceutical Research*, 32: 1626-1633.

de Viguerie, L., Duran, A., Bouquillon, A., Solé, V.A., Castaing, J., and Walter, P. (2009). Quantitative X-ray fluorescence analysis of an Egyptian faience pendant and comparison with PIXE. *Analytical and Bioanalytical Chemistry*, 395: 2219-2225.

Figueroa, R.G., Chávez, I.R., and Bonzi, E. (2014). *In vivo* EDXRF scanning analysis of human nail. *X-Ray Spectrometry*, 43: 338-344.

Fleming, D.E.B., Bennett, S.R., and Frederickson, C.J. (2018). Feasibility of measuring zinc in human nails using portable x-ray fluorescence. *Journal of Trace Elements in Medicine and Biology*, 50: 609-614.

Fleming, D.E.B., and Gherase, M.R. (2007). A rapid, high sensitivity technique for measuring arsenic in skin phantoms using a portable x-ray tube and detector. *Physics in Medicine and Biology*, 52: N459-N465.

Fleming, D.E.B., Gherase, M.R., and Anthonisen, M. (2013). Calibrations for measurement of manganese and zinc in nail clippings using portable XRF. *X-ray Spectrometry*, 42: 299-302.

Fleming, D.E.B., Nader, M.N., Foran, K.A., Groskopf, C., Reno, M.C., Ware, C.S., Tehrani, M., Guimarães, D., and Parsons, P.J. (2017). Assessing arsenic and selenium in a single nail clipping using portable X-ray fluorescence. *Applied Radiation and Isotopes*, 120: 1-6.

Fleming, D.E.B., and Ware, C.S. (2016). Portable X-ray fluorescence for the analysis of chromium in nail and nail clippings. Submitted to *Applied Radiation and Isotopes*, 121: 91-95.

Gherase, M.R., and Fleming, D.E.B. (2011). A calibration method for proposed XRF measurements of arsenic and selenium in nail clippings. *Physics in Medicine and Biology*, 56: N215-N225.

Guimarães, D., Praamsma, M.L., and Parsons, P.J. (2016). Evaluation of a new optic-enabled portable X-ray fluorescence spectrometry instrument for measuring toxic metals/metalloids in consumer goods and cultural products. *Spectrochimica Acta Part B*, 122: 192-202.

Hambidge, M. (2000). Human zinc deficiency. *Journal of Nutrition*, 130: 1344S-1349S.

Ichikawa, S., and Nakamura, T. (2016). Approaches to solid sample preparation based on analytical depth for reliable X-ray fluorescence analysis. *X-Ray Spectrometry*, 45: 302-307.

King, J.C., Brown, K.H., Gibson, R.S., Krebs, N.F., Lowe, N.M., Siekmann, J.H., and Raiten, D.J. (2016). Biomarkers of nutrition for development (BOND) – zinc review. *The Journal of Nutrition*, 146 (Supplement): 858S-885S.

McIver, D.J., VanLeeuwen, J.A., Knafla, A.L., Campbell, J.A., Alexander, K.M., Gherase, M.R., Guernsey, J.R., and Fleming, D.E.B. (2015). Evaluation of a novel portable X-ray fluorescence screening tool for detction of arsenic exposure. *Physiological Measurement*, 36: 2443-2459.

Pearce, D.C., Dowling, K., Gerson, A.R., Sim, M.R., Sutton, S.R., Newville, M., Russell, R., and McOrist, G. (2010). Arsenic microdistribution and speciation in toenail clippings of children living in a historic gold mining area. *Science of The Total Environment*, 408: 2590-2599.

Rodushkin, I., and Axelsson, M.D. (2000). Application of double focusing sector field ICP-MS for multielemental characterization of human hair and nails. Part II. A study of the inhabitants of northern Sweden. *Science of The Total Environment*, 262: 21-36.

Roy, C.W., Gherase, M.R., and Fleming, D.E.B. (2010). Simultaneous assessment of arsenic and selenium in human nail phantoms using a portable X-ray tube and a detector. *Physics in Medicine and Biology*, 55: N151-N159.

Solé, V.A., Papillon, E., Cotte, M., Walter, Ph., and Susini, J. (2007). A multiplatform code for the analysis of energy-dispersive X-ray fluorescence spectra. *Spectrochimica Acta Part B*, 62: 63-68.

Somervaille, L.J., Chettle, D.R., and Scott, M.C. (1985). *In vivo* measurement of lead in bone using x-ray fluorescence. *Physics in Medicine and Biology*, 30: 929-943.

Specht, A.J., Kponee, K., Nkpaa, K.W., Balcom, P.H., Weuve, J, Nie, L.H., and Weisskopf, M.G. (2018). Validation of x-ray fluorescence measurements of metals in toenail clippings against inductively coupled plasma mass spectrometry in a Nigerian population. *Physiological Measurement,* 39: 085007 (9 pp).

Studinski, R.C.N., McNeill, F.E., Chettle, D.R., and O'Meara, J.M. (2005). Estimation of a method detection limit for an *in vivo* XRF arsenic detection system. *Physics in Medicine and Biology*, 50: 521-530.

Wessells, K.R., and Brown, K.H. (2012). Estimating the global prevalence of zinc deficiency: results based on zinc availability in national food supplies and the prevalence of stunting. *PLoS One*: e50568.

Figures

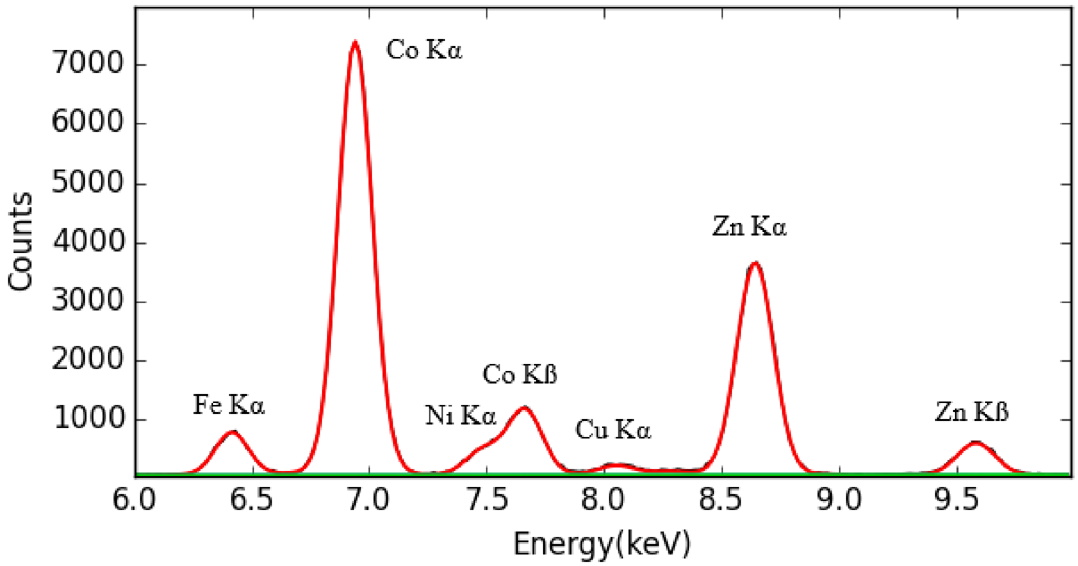

(a)

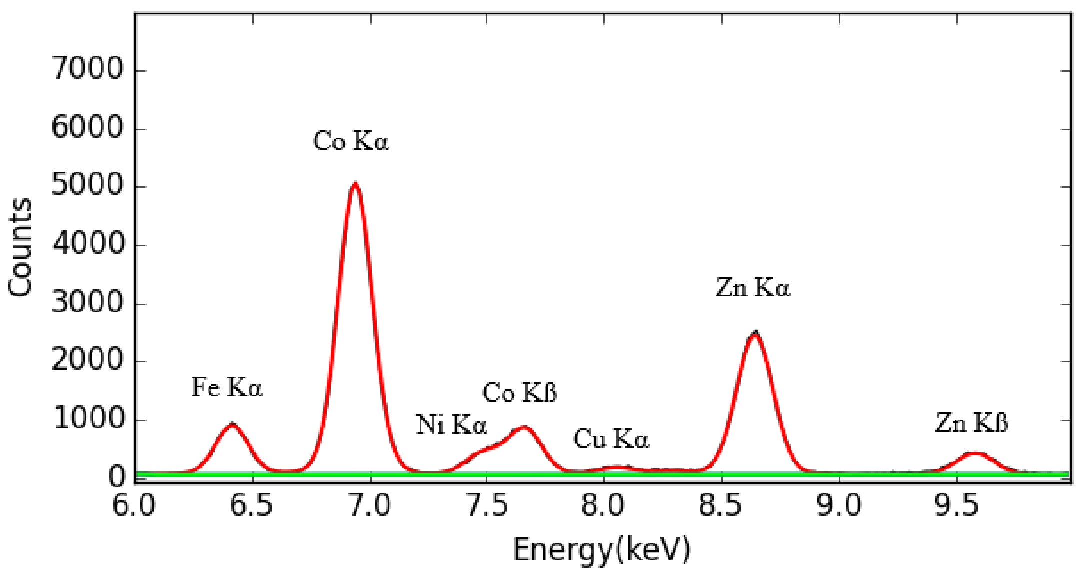

(b)

Figure 1. (a) Energy spectrum obtained from 300 s measurement of clipping # 5, with data fit by PyMca software. **(b)** Energy spectrum obtained from 300 s measuremnt of clipping # 8, with data fit by PyMca software. In both cases, the red line represents the PyMca fit for various elements, while the green line represents the background continuum. The data points are shown in black and are mostly obscured by the PyMca fitting. The zinc Kα peak is centered at 8.6 keV and the zinc Kβ peak is centered at 9.6 keV.

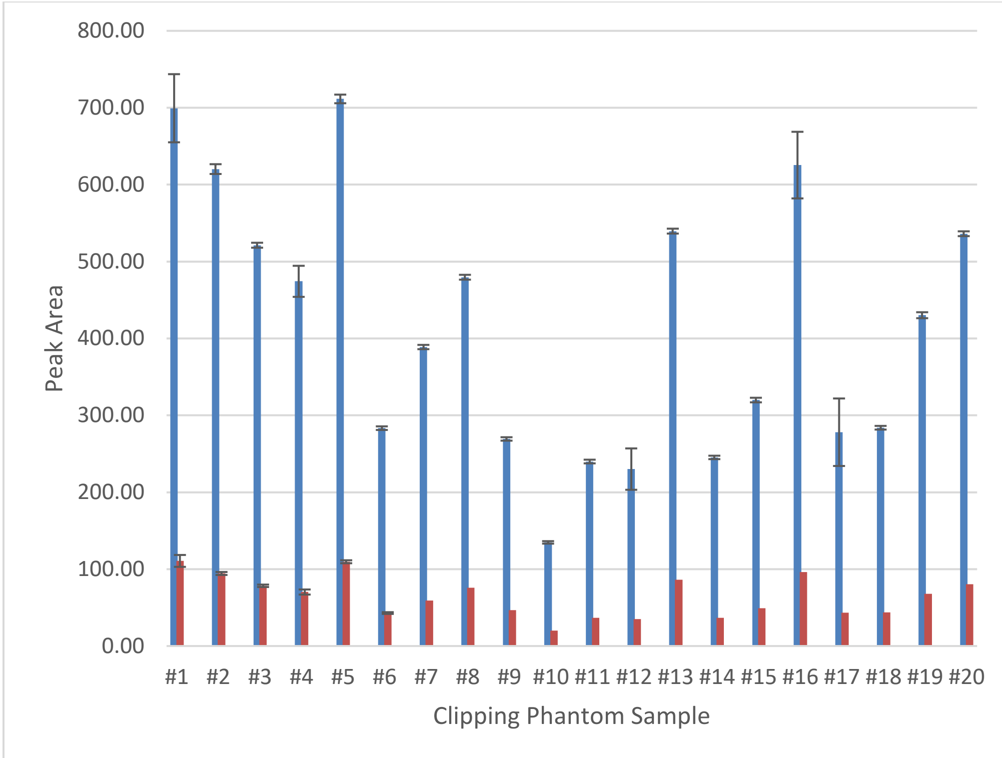

Figure 2. PyMca fitting results for peak area from zinc Kα (blue) and zinc Kβ (red) for each of the twenty clipping phantoms. Uncertainty bars, also taken from the PyMca output, are indicated for each area.

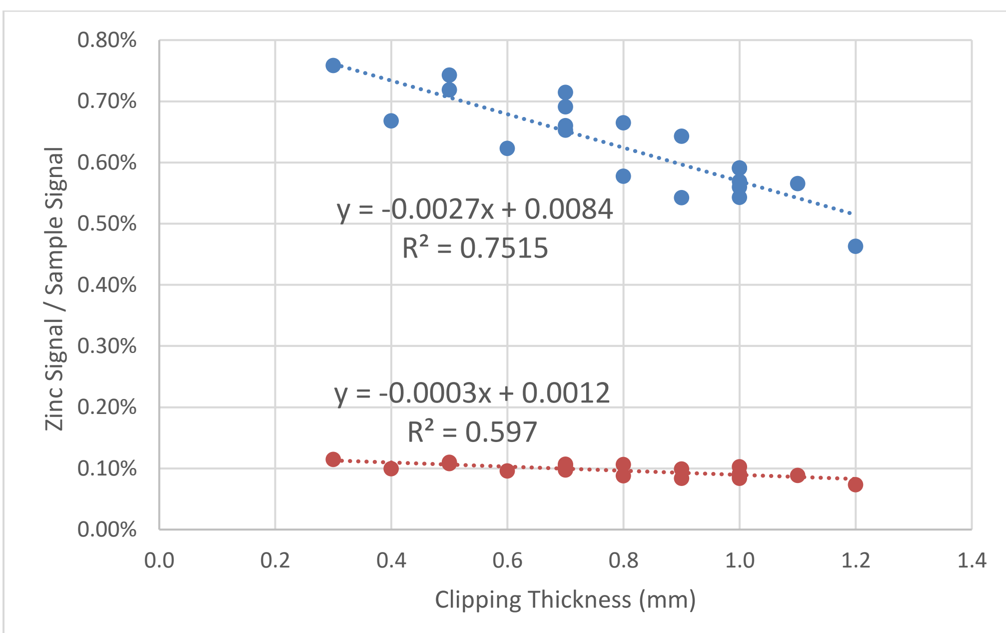

Figure 3. The ratio of zinc signal / sample signal is shown as a function of clipping thickness for both the zinc Kα (blue) and zinc Kβ (red) signals. The best fit linear relationships between the variables are dispalyed next to their respective data sets.

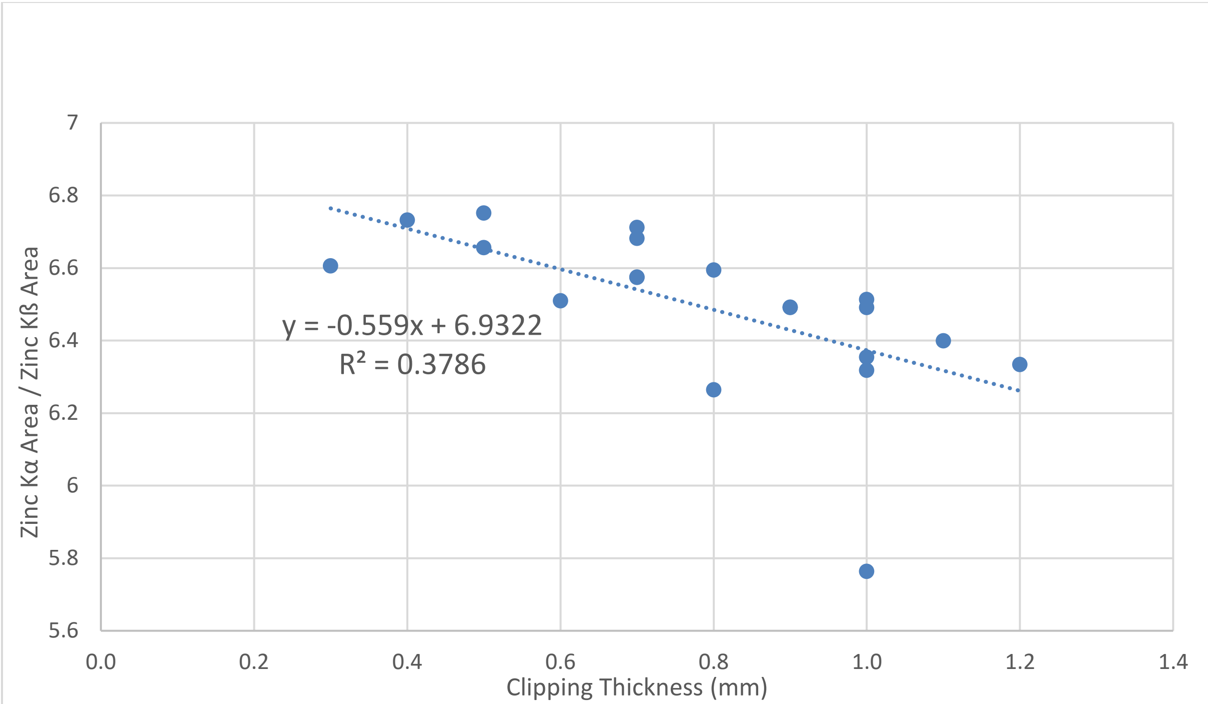

Figure 4. The ratio of zinc Kα area / zinc Kβ area is shown as a function of clipping thickness. The best fit linear relationship between the variables is also dispalyed.